Titanium-Based Anode Materials for Safe Lithium-Ion Batteries

Zonghai Chen, Ilias Belharouak, Y.-K. Sun, and Khalil Amine**

Lithium-ion batteries have been long considered a promising energy storage technology for electrification of the transportation system. However, the poor safety characteristics of lithium-ion batteries is one of several technological barriers that hinder their deployment for automobile applications. Within the field of battery research and development, titanium-based anode materials have recently attracted widespread attention due to their significantly better thermal stability than the conventional graphite anode. In this chapter, the fundamental properties and promising electrochemical performance of titanium-based anode materials will be discussed for applications in hybrid electric vehicles.

1. Introduction

Among the currently available energy storage technologies, the lithium-ion battery has the highest energy density and, hence, has received intense attention from both the academic community and industry as the power source in hybrid electric vehicles (HEVs), plug-in hybrid electric vehicles (PHEVs), and full electric vehicles (EVs).[1,2] However, the large-scale deployment of lithium-ion batteries to power HEVs, PHEVs, and EVs is significantly hindered by several major technological barriers, including high cost, insufficient life, intrinsically poor safety characteristics, and poor low-temperature performance (<–20 °C). In particular, the cost of the battery pack to power vehicles will be the major deciding factor to entice consumers to purchase PHEVs, HEVs, or full EVs. In the case of full EVs, the cost of the battery pack can be significantly compensated for by the elimination of the internal combustion engine. However, the energy-demanding full-EV application requires a very high-performance battery to store enough energy for long driving distance (>100 miles). The energy density of such a battery pack should be at least double that of state-of-the-art lithium-ion technology so that a reasonable-size battery can be manufactured to meet the high energy demand of the full EV. An alternative to the full EV is the PHEV, in which a battery with a high energy density and high power capability as well as an electric motor will be added to a vehicle with a small internal combustion engine. In this case, the battery pack provides energy for full electric driving for a reasonable distance (10–40 miles). When the battery pack is drained to a certain level, the vehicle will operate in regular HEV mode, relying on gasoline for energy and using the battery to improve the energy utilization efficiency. In contrast to the full EV, the cost of the internal combustion engine remains, and hence, the PHEV cost can be substantially higher than that of conventional vehicles using internal combustion engines. It is physically and economically more practical to develop lithium-ion batteries for the HEV, which only requires a small high-power battery to frequently store/deliver a small amount of energy during braking, accelerating, and starting the vehicle. After about one decade of continuous development, there have been several reported cell chemistries[3,4] (e.g., graphite/$LiNi_{0.8}Co_{0.15}Al_{0.05}O_2$, graphite/$LiFePO_4$, graphite/$Li_{1+x}Mn_{2-x}O_4$, and $Li_4Ti_5O_{12}$/$Li_{1+x}Mn_{2-x}O_4$) that can meet the power, life, and cost requirements for the HEV battery,[5] while a battery technology to meet the requirements of PHEVs and EVs is still under development.

The safety issue is another major barrier that hinders the deployment of lithium-ion batteries in automobiles. In a fully charged graphite/$LiMO_2$ (M = transition metal) cell, the cathode is composed of a strongly oxidative transition metal oxide, and the anode is mainly LiC_6, which has similar chemical reactivity to the lithium metal. Sandwiched between them is a non-aqueous electrolyte, typically a solution of $LiPF_6$ in a mixture solvent of ethylene carbonate and ethyl methyl carbonate, which can be both oxidized and reduced in the wide working potential window of lithium-ion batteries. Triggering the reaction between the cathode and the electrolyte or between the anode and the electrolyte generally leads to the release of a large amount of heat during a short period of time, potentially leading to fire or explosion of the battery (also called "thermal runaway"). The cause has been widely attributed to the thermal instability of the delithiated cathode ($Li_{1-x}MO_2$), which starts to decompose at above 200 °C and generates a large amount of heat, sometimes larger than that generated from an equivalent amount of the lithiated graphite (Li_xC_6).[6,7] However, more attention should be paid to the anode side from the safety perspective, because the solid-electrolyte interphase (SEI) on the graphite surface tends to decompose at a temperature as low as 60 °C.[8] The SEI layer is an organic/inorganic composite thin film that is formed during the initial intercalation of

Dr. Z. H. Chen, Dr. I. Belharouak, Dr. K. Amine
Chemical Sciences and Engineering Division
Argonne National Laboratory
9700 South Cass Avenue, Lemont, IL 60439, USA
E-mail: amine@anl.gov
Dr. Y.-K. Sun
Department of WCU Energy Engineering
Hanyang University
Seoul 133-791, South Korea
E-mail: yksun@hanyang.ac.kr

DOI: 10.1002/adfm.201200698

lithium into graphite at about 0.8 V, and that suppresses the continuous chemical reaction between lithiated graphite and the electrolyte.[9] When the battery is exposed to a temperature above its critical temperature, the SEI layer will decompose and directly expose lithiated graphite to the non-aqueous electrolyte, resulting in a continuous exothermal reaction between the lithiated graphite and the electrolyte.[10] The continuous heat flow from the reaction can slowly raise the internal temperature of the battery and eventually trigger the major reaction of the cathode at about 200 °C. Therefore, the thermal stability of the SEI is critical to the safety of lithium-ion batteries using graphite as the anode.

Titanium-based materials are a class of alternative materials to graphite that operate at a potential above 0.8 V vs. Li^+/Li, where an stable SEI layer is not required. It has been consistently reported that titanium-based anode materials can offer a significant safety advantage over the graphite anode, and many researchers are attempting to develop high power, long life, and extremely safe lithium-ion chemistries with titanium-based anode materials for HEV applications. In this article, particular attention will be paid to the structure, electrochemical performance, and safety of $Li_4Ti_5O_{12}$,[4,11–16] TiO_2,[17–23] and $MLi_2Ti_6O_{14}$(M = Sr, Ba, and Na)[24–26] for potential applications in HEVs.

Khalil Amine is a senior scientist and manager of the Advanced Lithium Battery Technology group at Argonne National Laboratory. He earned his master's degree in chemistry and his PhD degree in materials science from the University of Bordeaux, France. His research interest includes advanced materials and battery systems for HEV, PHEV, EV, satellite, military and medical applications.

2. $Li_4Ti_5O_{12}$

The synthesis and characterization of $Li_{3+y}Ti_{6-y}O_{12}$ spinels ($0 \le y \le 1$) have been under investigation since the 1970s due to their superconductivity at a relatively high transition temperature.[27] The reversible insertion/removal of lithium into $Li_4Ti_5O_{12}$ was reported about a decade later.[28] Solid-state synthesis is generally used for the preparation of $Li_4Ti_5O_{12}$ because of its simplicity, low cost, and well-grown crystals at relatively high sintering temperature (800–1000 °C). TiO_2 is widely used as the titanium source for this approach, and the typical lithium source can be either LiOH or Li_2CO_3; TiO_2 is mixed with an equivalent amount of lithium source, and the mixture is then sintered at high temperature (800–1000 °C) for 8–12 hours.[12,14,16] The $Li_4Ti_5O_{12}$ obtained from this solid-state synthesis is an electronic insulator with well-grown, large primary particles. Lithium cells with $Li_4Ti_5O_{12}$ anodes composed of micro-sized particles, whose theoretical capacity is 175 mAh/g, generally deliver a specific capacity of about 100 mAh/g and have poor rate capability.[28] It was believed that the electrochemical performance of $Li_4Ti_5O_{12}$ could be dramatically improved by carefully controlling the particle size of the final active materials to shorten the diffusion length of the lithium/electron inside the particle. Aldon et al.[29] reported that this goal can be easily accomplished by a sol-gel method. In this method, both soluble titanium salt and lithium salt are added to a solvent like ethanol to form a precursor gel, and the solvent is then evaporated to obtain nano-sized precursor particles, which are then annealed at 800–100 0 °C to obtain the final $Li_4Ti_5O_{12}$ powder. It has been reported that nanometer-size materials can approach their theoretical specific capacity and result in good rate capability.[4] However, the energy density for batteries using nanometer-sized $Li_4Ti_5O_{12}$ anode materials remains problematic for two reasons. First, $Li_4Ti_5O_{12}$ operates at 1.55 V vs. Li^+/Li, which is about 1.5 V higher than the operating voltage of graphitic anodes. Second, high porosity and low loading density are expected for electrodes using nanometer-size particles and can lead to further reduction in volumetric energy density of the battery.

A practical approach to increase the loading density of the $Li_4Ti_5O_{12}$ electrode is to synthesize materials consisting of micrometer-sized secondary particles composed of nanometer-sized primary particles (see **Figure 1**b for an exemplary scanning electron microscopy image illustrating this morphology);[4] the micrometer-sized particles improve the tap density and the load density of the electrode, while the nanometer-sized primary particles maintain all the benefits associated with nano $Li_4Ti_5O_{12}$ powders. In this approach, $TiCl_4$ or other soluble titanium salt is used as the starting material to prepare the porous $TiO_2 \cdot 2H_2O$ precursor. During the high temperature sintering, the porous structure in the precursor is maintained, and the removal of the crystalline water in the precursor during material synthesis helps to maintain a percolated tunnel structure inside the particle; this tunnel structure will uptake non-aqueous electrolyte after the cell is assembled and will increase the accessibility of $Li_4Ti_5O_{12}$ toward lithium ions.

A further modification of the synthesis method is to add a carbon source like pitch to the starting material, e.g., a mixture

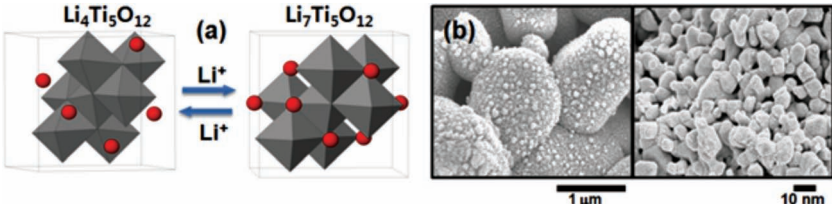

Figure 1. (a) Structure of $Li_4Ti_5O_{12}$ and $Li_7Ti_5O_{12}$ showing no volume change after charge and discharge.[4] (b) Scanning electron microscopy under low and high magnification of nanostructured $Li_4Ti_5O_{12}$ with micrometer-sized secondary particles and nanometer-sized primary particles. Reproduced with permission.[4]

of mesoporous TiO_2, LiOH, and pitch.[13] During the sintering process, the added carbon source maintains the reducing environment, decomposes at a high temperature, and generates a carbon coating layer on the surface of the final $Li_4Ti_5O_{12}$; the carbon coating can then enhance the electronic conductivity of the materials and further improve the rate capability of lithium-ion batteries using carbon-coated $Li_4Ti_5O_{12}$ anodes.

The $Li_4Ti_5O_{12}$ anode material has a spinel structure of space group $Fd\bar{3}m$, whose unit cell contains eight formula units of $(Li)^{8a}(Li_{1/3}Ti_{5/3})^{16d}O_4{}^{32e}$, in which the 8a tetrahedral sites are fully occupied by lithium, the 16d octahedral sites are shared between lithium and titanium with an atomic ratio of 1:6, and the 32e sites are filled with oxygen atoms (see Figure 1a). One formula unit of $Li_4Ti_5O_{12}$ has the capability to reversibly uptake up to 3 lithium atoms to deliver a theoretical capacity of 175 mAh/g, converting to a rock salt structure $Li_7Ti_5O_{12}$ (see Figure 1b). The phase transformation from the spinel to rock salt structure only results in slight shrinkage of the lattice parameter, from 8.3595 Å to 8.3538 Å, with only 0.2% change in the cell volume. Therefore, the $Li_4Ti_5O_{12}$ material is widely considered as zero strain for lithium insertion, and extremely long cycle life for lithium insertion/removal is expected because its small lattice change can help to maintain the structural stability of $Li_{4+x}Ti_5O_{12}$ and the mechanical integrity of the binder/carbon black matrix that holds the $Li_{4+x}Ti_5O_{12}$ particles together with a good electron conducting pathway to the current collector.

The electrochemical insertion of lithium atoms into $Li_4Ti_5O_{12}$ is a two-phase process that forms a solid solution between $Li_4Ti_5O_{12}$ and $Li_7Ti_5O_{12}$, and that presents as a long voltage plateau at 1.55 V vs. Li^+/Li. Worth mentioning is that three lithium atoms in $Li_4Ti_5O_{12}$ occupy 8a tetrahedral sites, and that no lithium is present in the 8a sites of $Li_7Ti_5O_{12}$. The three 8a lithium atoms migrate to the 16c sites during the insertion process, and the newly inserted lithium atoms fill the remaining 16c sites.[29–31] The migration of lithium atoms from 8a to 16c sites is driven by the coulombic repulsion from the inserted lithium atoms in the 16c sites, whose distance to the nearby 8a sites is only 1.81 Å. The kinetics of lithium migration between 8a and 16c sites, which is determined by the energy barrier between them, can hinder the insertion process. The thermal migration of lithium from 8a to 16c sites in $Li_4Ti_5O_{12}$ without extra inserted lithium (or no repulsion force) was observed at about 700 °C.[30] This high energy barrier for lithium migration can lead to the co-occupation of 8a and 16c sites when fast insertion occurs. Therefore, reduced reversible capacity and low rate capability are generally reported for micrometer-sized $Li_4Ti_5O_{12}$ materials, in which the co-occupation of 8a and 16c sites is not energetically favored. Borghols et al.[31] suggested that the boundary effect of materials with large specific surface area can help to relax the repulsion force and make it easier for co-occupation of 8a and 16c sites in the near surface region. This suggestion agrees well with the strategies to develop nanometer-sized or nano-structured materials to maximize their electrochemical performance.

An indirect support for the hypothesis of 8a-16c site co-occupation is that the chemical lithiation of $Li_4Ti_5O_{12}$, which is much faster than the electrochemical process, resulted in only a small degree of 8a site lithium migrated into 16c sites, and the majority of the inserted lithium was irreversibly trapped in 48f sites.[29] It was also reported that more lithium could be electrochemically inserted into $Li_7Ti_5O_{12}$ when a potential below 1.0 V vs. Li^+/Li was applied.[15,30] However, a large hysteresis was observed in the voltage profile within the window below 1.5 V, probably due to the repulsion force between lithium in the 16c and 8a sites.

In a practical lithium-ion cell, the capacity of the anode is generally not less than that of the cathode to avoid the lithium plating on the anode side when the cell is fully charged. Therefore, the reversible capacity of the cell is determined by the amount of the accessible lithium in the cathode material; any side reactions that can consume either lithium or charge/electron will directly contribute to the capacity loss of the cell.[32,33] One of the sources that continuously consume lithium is the decomposition/formation of the SEI layer on the graphite surface at elevated temperatures (≥60 °C).[10,33] This consumption will become worse when the graphitic anode is paired with a lithium transition metal oxide/phosphate cathode because the migration of a trace amount of transition metal from the cathode side to the anode side could have a detrimental impact on the thermal stability of the SEI layer and accelerate the side reaction between the lithiated anode and the non-aqueous electrolyte, accelerating the capacity fade at elevated temperatures.[34] Alternatively, $Li_4Ti_5O_{12}$ operates at a higher potential (~1.55 V), where an SEI layer is not required. Therefore, the consumption of valuable lithium to form the SEI layer as well as the negative impact of migrated transition metals can be dramatically reduced. In addition, the intrinsic zero strain during lithium insertion/removal is another major contributor to the superior electrochemical performance of $Li_4Ti_5O_{12}$ over graphitic anodes.

Figure 2a shows the charge/discharge profile of a half cell with a conventional $Li_4Ti_5O_{12}$ electrode with micrometer-sized particles. The cell was discharged at a 1C rate to reach full insertion of lithium into the working electrode material. Then, the cell was charged to 3.0 V using different rates (1C, 10C, and 20C). At the 1C rate, the cell delivered a specific capacity of about 120 mAh/g. The charge capacity decreased to about 80 mAh/g at 20C, with a large hysteresis loop in the voltage profile due to the difficulty in lithium migration between 8a and 16c sites in bulk materials (see above). Figure 2b shows the charge/discharge profile of a half cell using specially designed $Li_4Ti_5O_{12}$ with micrometer-sized secondary particles and nanometer-sized primary particles. The testing procedure was identical to the one used for the results shown in Figure 2a. The nano-structured $Li_4Ti_5O_{12}$ delivered a very high reversible capacity (>160 mAh/g for all three rates), and capacity retention was very high when the cell was charged at the 20C rate.

Figure 2c shows the discharge capacity vs. cycle number of half cells using carbon-free and carbon-coated $Li_4Ti_5O_{12}$ tested with different charge and discharge rates. The benefit of carbon coating on the electrochemical performance of $Li_4Ti_5O_{12}$ is clearly evident. The discharge capacity of carbon-free $Li_4Ti_5O_{12}$ dropped dramatically with increasing discharge rate. The capacity was very low (18 mAh/g) at the 10C rate. For the carbon-coated $Li_4Ti_5O_{12}$, the rate capability strongly depended on the amount of coated carbon, especially at high rates. The

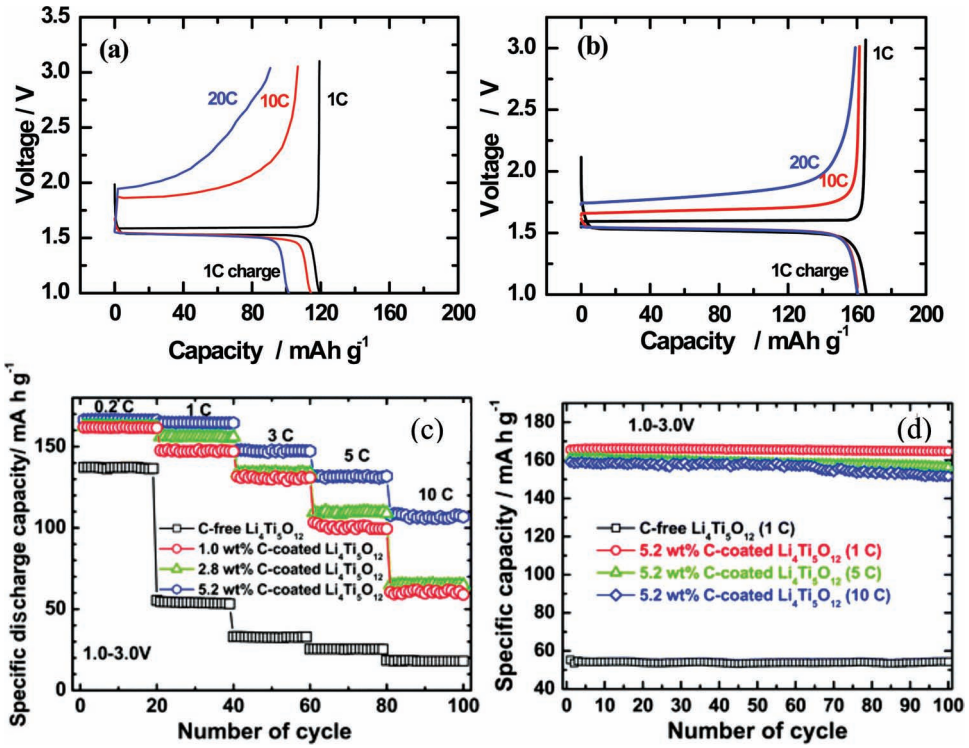

Figure 2. Charge and discharge curves of (a) micrometer-size $Li_4Ti_5O_{12}$ and (b) nano-structured $Li_4Ti_5O_{12}$ with micrometer-sized secondary particles and nanometer-sized primary particles. The test was carried out in half cell. Initially, half cells were charged and discharged at 0.2C rate, and then they were charged at 1C rate and discharged at different rates. Reproduced with permission.[4] (c) Rate capability of carbon-free and carbon-coated $Li_4Ti_5O_{12}$ from 0.2C rate (0.34 mA/g) to 10C rate (1.7 A/g).[13] (d) Cyclability of 5.2 wt% carbon-coated $Li_4Ti_5O_{12}$ from 1C rate (0.17 A/g) to 10C rate (1.7 A/g) in comparison with carbon-free $Li_4Ti_5O_{12}$ cycled at 1C rate (0.15 A/g). Reproduced with permission.[13] Copyright 2011, The Royal Society of Chemistry.

increase in the amount of coated carbon on $Li_4Ti_5O_{12}$ particles led to a noticeable enhancement in rate capability. If the capacity obtained at C/5 is used as a standard, the capacity retention at the 10C rate is 37%, 40%, and 65% for anodes with 1.0, 2.8, and 5.2 wt% carbon coating, respectively. Figure 2d shows the capacity retention of a half cell with the $Li_4Ti_5O_{12}$ electrode having 5.2 wt% coated carbon tested at the 1, 5, and 10C rates over 100 cycles, as well as another half cell using carbon-free $Li_4Ti_5O_{12}$ cycled at 1C rate as a control. The reversible capacity for the carbon-coated $Li_4Ti_5O_{12}$ was about 160 mAh/g throughout the whole cycling test, even though the applied current was increased to the 10C rate (1.7 A/g). Meanwhile, the carbon-free $Li_4Ti_5O_{12}$ had a low reversible capacity of 54 mAh/g at the 1C rate. These test results indicate that the carbon-coated $Li_4Ti_5O_{12}$ is sufficiently stable for high-rate cycling.

The performance advantage of nanometer-sized or nano-structured $Li_4Ti_5O_{12}$ over graphitic anodes can be clearly demonstrated when they are paired with lithium transition metal oxides to form a full cell configuration. **Figure 3**a compares the capacity retention of two full cells using $Li_{1+x}Mn_{2-x}O_4$ (LMO) as the cathode material over extended cycling tests. The anode was either carbon or nano-structured $Li_4Ti_5O_{12}$ with micrometer-sized secondary particles and nanometer-sized primary particles (MSNP-LTO). To accelerate the cycle life test, the cells were charged and discharged at high current density (5C) and at high temperature (55 °C). The MSNP-LTO/LMO cell showed no capacity fade after 1000 cycles under these aggressive test conditions, while the carbon/LMO cell lost more than 25% capacity under the same test conditions. In the carbon/LMO cell, the capacity fade was attributed to manganese migration from the cathode to the anode side that compromised the integrity of the SEI layer. In contrast, no SEI layer was required for the MNSP-LTO electrode because of its high stability in the charged state and its high operating voltage (1.5 V vs. Li^+/Li). Figure 3b compares the power fade vs. aging time of MSNP-LTO/LMO and carbon/LMO cells. Both cells were aged at 60% state of charge (SOC) and at 55 °C for 8–10 weeks. The carbon/LMO cell showed poor calendar life, with over 38% power fade after only eight weeks, mainly caused by the interfacial impedance rise at the carbon anode. In contrast, the MSNP-LTO/LMO cell showed a small initial power fade (less than 4%) during the first four weeks. Thereafter, the power fade stabilized at about 7% after 10 weeks. Similar results were also reported for $Li_4Ti_5O_{12}$-based full cells having other cathode materials with higher energy density than $Li_{1+x}Mn_{2-x}O_4$. For instance, Jung et al.[17] investigated the electrochemical performance of a full cell using carbon-coated $Li_4Ti_5O_{12}$ as the anode and $Li[Ni_{0.45}Co_{0.1}Mn_{1.45}]O_4$ as the cathode (a 4.7 V high-voltage spinel), and reported that the cell when cycled at 1C for 500 cycles at room temperature maintained an excellent capacity retention of 85.4%.

Figure 3c compares the area specific impedance (ASI) for MSNP-LTO/LMO, micrometer-sized LTO/LMO, and carbon/

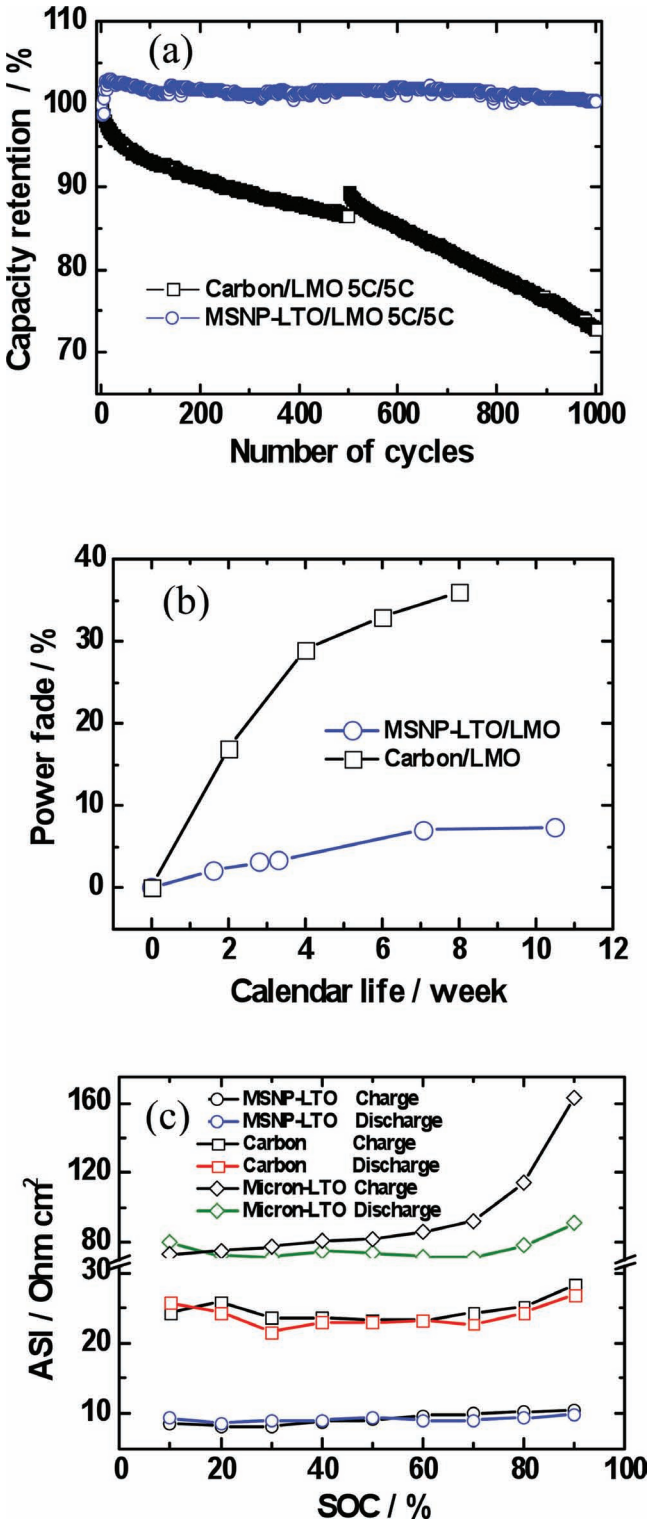

Figure 3. (a) Capacity retention during cycling at 55 °C of MSNP-LTO/LMO and carbon/LMO cells; both cells were charged and discharged at 5C rate.[4] (b) Power fade vs. aging time at 55 °C of MSNP-LTO/LMO and carbon/LMO cells. The power of each cell was determined from the hybrid pulse power characterization test.[4] (c) Area specific impedance vs. state of charge of MSNP-LTO/LMO, carbon/LMO, and micrometer-size LTO/LMO cells. Reproduced with permission.[4]

LMO cells that were tested using the hybrid power performance characteristics (HPPC) testing procedure proposed by the Partnership of Next Generation Vehicles (PNGV). Hybrid electric vehicles require very high charge and discharge pulse power for vehicle acceleration and regenerative braking. To meet the 25-kW pulse power requirement in HEVs, the ASI of the cell must be less than 35 ohm cm^2. These values were then used to determine the energy swings within the limits of the required pulse power capability. For the MSNP-LTO/LMO cell, the ASI values were around 9 ohm cm^2, about one-eighth the ASI values for the cell with LTO anodes composed of 8-μm particles (80 ohm cm^2). Moreover, the ASI values for the MSNP-LTO/LMO cell were one-fourth of the upper ASI limit to power an HEV and were almost one-third of the ASIs for the conventional carbon/LMO system. In addition, the pulse-power test of the cells at −30 °C showed that the MSNP-LTO/LMO could meet the 5-kW requirement during the cold cranking test, while the carbon/LMO cell failed.[4]

Figure 4 compares the differential scanning calorimetry (DSC) profiles of lithiated carbon and lithiated LTO with the presence of the non-aqueous electrolyte.[11] The results show that the fully lithiated graphite anode generated much more heat than the fully lithiated $Li_{6.9}Ti_5O_{12}$ anode (2750 vs. 383 J/g, respectively). In the case of lithiated graphite, the thermal degradation of the SEI layer occurred at around 100 °C, leading to a wide exothermal reaction because of the continuous decomposition/formation of the SEI layer. This exothermal reaction was much reduced for the $Li_{6.9}Ti_5O_{12}$, because the SEI layer may not have been formed upon lithiation of $Li_4Ti_5O_{12}$ at the higher operating potential. In summary, the thermal characteristics of $Li_{4+x}Ti_5O_{12}$ phases are significantly better compared to those of lithiated graphite (i.e., higher onset temperature and much less generated heat, as shown in the accumulated heat curve in **Figure 5**b).

Lu et al.[14] reported that substantial heat could also be generated during normal high rate operation of lithium-ion batteries. This heat generation can be even worse in a large battery pack, where the thermal management system will be less efficient at removing heat from the battery than that for a small pack. Figures 5a and 5b show the heat profiles of LTO/$Li_{1+x}Mn_{2-x}O_4$ cell and mesocarbon microbeads (MCMB)/$Li_{1+x}Mn_{2-x}O_4$ cells during charge at 0.1 mA (C/10) and 1.0 mA (1C), respectively. The heat flow was measured by isothermal micro-calorimetry. For both charge rates, the heat release of the MCMB/$Li_{1.156}Mn_{1.844}O_4$ cell is larger than that of the LTO/$Li_{1.156}Mn_{1.844}O_4$ cell. Figure 5c shows the total heat generation of LTO/$Li_{1.156}Mn_{1.844}O_4$ and MCMB/$Li_{1.156}Mn_{1.844}O_4$ cells during the charge process as a function of the charge rates. Clearly, the total heat generation of the cell with the LTO anode is smaller than that with the MCMB anode. This result indicates that the LTO/$Li_{1.156}Mn_{1.844}O_4$ cell has less heat generation and better safety characteristics.

Amine et al.[4] also demonstrated the unmatched safety characteristics of LTO-based lithium batteries in large format pouch cells after nail penetration and overcharge abuse, the most severe abuse conditions for lithium-ion batteries. **Figures 6**a and 6b show the nail penetration test results for a carbon/LMO cell and an MSNP-LTO/LMO cell, respectively. Both cells were fully charged before testing. Once the

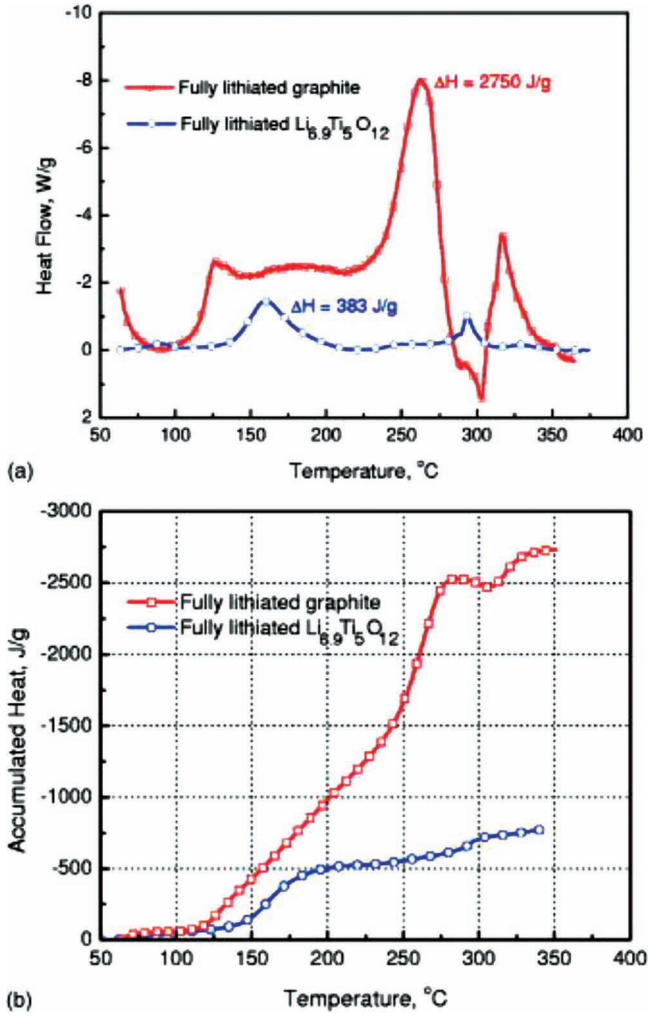

Figure 4. (a) Differential scanning calorimetry curves of fully lithiated graphite and fully lithiated $Li_4Ti_5O_{12}$.[11] (b) Corresponding accumulated heat curves. Reproduced with permission.[11] Copyright 2004, The Electrochemical Society.

nail penetrated the carbon/LMO cell, the cell temperature increased dramatically to 150 °C, caused by internal short and reaction of the non-aqueous electrolyte with the charged electrode materials. In contrast, the MSNP-LTO/LMO cell showed only a 5 °C increase in the cell temperature after nail penetration, clearly indicating outstanding abuse tolerance. Other battery systems based on carbon anodes and $LiNi_{0.8}Co_{0.15}Al_{0.05}O_2$ or $LiFePO_4$ cathodes also show larger thermal events than the MSNP-LTO/LMO system. Figure 6c shows the temperature profile of a 4-V carbon/LMO cell that was overcharged to 12 V. After about 45 min, the cell temperature increased significantly and reached over 500 °C, followed by an explosion. When the 2.5 V MSNP-LTO/LMO cell was overcharged to 15 V, the cell temperature after overcharge reached only 80 °C, with no explosion or thermal runaway (Figure 6d). In fact, the cell was able to operate normally after this severe overcharge test.

3. TiO_2

Within the oxide family, titanium dioxide (TiO_2, titania) is one of the most studied members because of its abundance and structural diversity. It is also well known for its wide spectrum of applications, including pigments, sunscreen and UV-absorber, photovoltaics, photocatalysts, electronic data storage medium, cost-effective protein splitting, and the anode material for lithium-ion batteries. Titania occurs in nature as well-known minerals like rutile (tetragonal, $P4_2/mnm$), anatase (tetragonal, $I4_1/amd$), and brookite (orthorhombic, $Pbca$). Among these, rutile TiO_2 is the equilibrium component at most temperatures, and metastable phases like anatase and brookite will thermodynamically convert to rutile at high temperature. As shown in **Figure 7**, their structures are all built upon the connection of TiO_6 octahedra with different corner- and edge-sharing configurations. TiO_2 with different structures can be prepared by various approaches, including a template-assisted method,[35] sol-gel process,[36] electrochemical anodic oxidation,[37] and hydrothermal process.[38] In addition to three naturally occurred forms, TiO_2 has several synthetic forms like TiO_2(B) (monoclinic, $C2/m$), TiO_2(H) (tetragonal, hollandite-like form), TiO_2(R) (orthorhombic, ramsdellite-like form), TiO_2(II) (orthorhombic, α-PbO_2-like form), baddeleyite-like form (monoclinic, 7-coordinated titanium), TiO_2-OI (orthorhombic), cubic form, and TiO_2-OII (orthorhombic, cotunnite($PbCl_2$)-like).

Various forms of TiO_2[17] can be an ideal host for reversible lithium insertion/removal and, hence, are promising anode materials for lithium-ion batteries. In theory, TiO_2 can host up to 1 mol of lithium and deliver a theoretical capacity of 330 mAh/g (corresponding to the composition $LiTiO_2$). However, unlocking this theoretical value has been proven very challenging. Dambournet et al.[20] deployed a pair distribution function (PDF) technique to study the structure of lithiated brookite-TiO_2, and found that brookite-TiO_2 can host up to 0.75 mol lithium, corresponding to the composition $Li_{0.75}TiO_2$. In $Li_{0.75}TiO_2$ (brookite), lithium was suggested to occupy the 8c site within a distorted octahedral structure. One of the Li-O bonds in the LiO_6 octahedra is much longer (~2.5 Å) than the others, with an average Li-O distance of 2.0 Å. Armstrong et al.[39] investigated lithium insertion into TiO_2(B) and found that the inserted lithium preferred to occupy the square planar site in the [010] channel (the C site[40] or 4g site, see **Figure 8**) at low lithium concentration ($x < 0.25$ in Li_xTiO_2(B)). Further insertion of lithium into Li_xTiO_2(B) ($0.25 < x < 0.5$) made the C site energetically unfavored, so that the lithium in the C site (or 4g site) migrated with the inserted lithium into the five-coordinated A1 site (4i, see Figure 8). Within the high lithium concentration range ($0.5 < x < 1$ for Li_xTiO_2(B)), lithium occupied the A1 and A2 sites. **Figure 9** schematically shows the phase transformation of rutile TiO_2 during the lithium insertion.[41] During the initial insertion ($0 < x < 0.5$ for Li_xTiO_2), rutile TiO_2 crystalline particles gradually convert from initial tetragonal symmetry ($P42/mnm$) toward a new phase that is indexed with the monoclinic space group 10 ($P2/m$), which is very similar to the initial $P42/mnm$ structure. Within the high lithium concentration range ($0.5 < x < 0.85$ for Li_xTiO_2), significant crystal structure change occurs when the monoclinic $P2/m$ structure converts into the layered $P2/m$

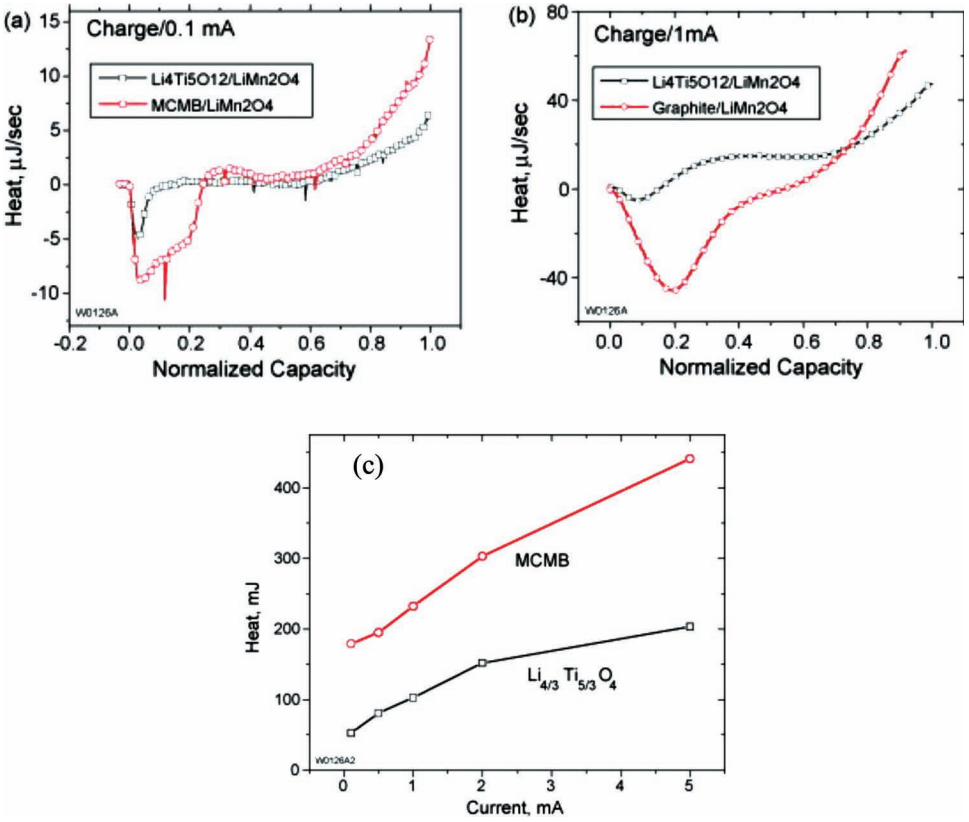

Figure 5. Heat flow profiles of $Li_4Ti_5O_{12}/Li_{1.156}Mn_{1.844}O_4$ and MCMB/$Li_{1.156}Mn_{1.844}O_4$ cells as a function of normalized capacity at (a) 0.1 mA and (b) 1 mA charge rate; (c) total heat generation of $Li_4Ti_5O_{12}/Li_{1.156}Mn_{1.844}O_4$ and MCMB/$Li_{1.156}Mn_{1.844}O_4$ cells during the charge process as a function of the charge rate. Reproduced with permission.[14] Copyright 2007, Elsevier.

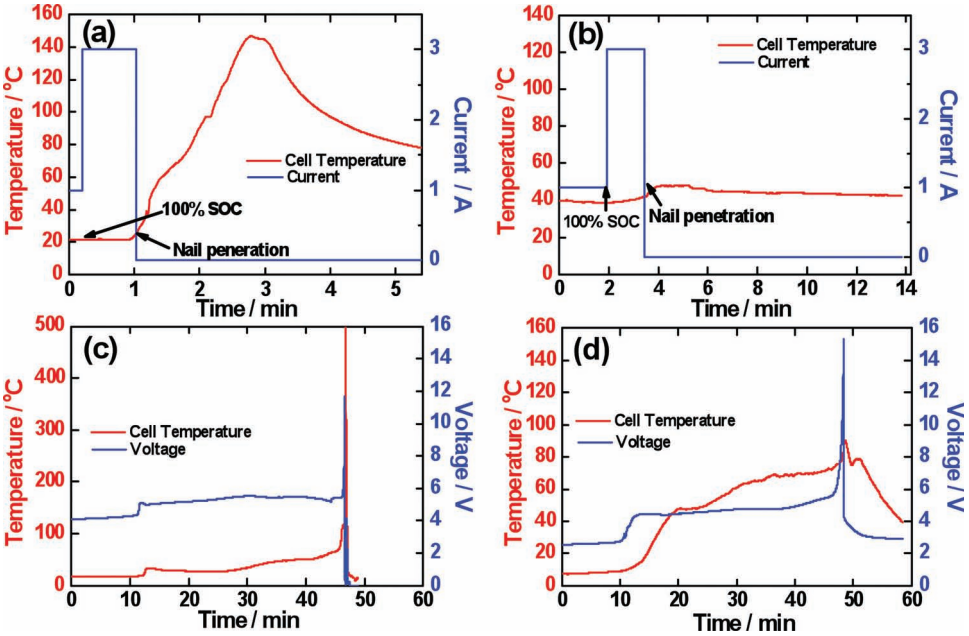

Figure 6. Nail penetration test showing surface temperature of fully charged (a) carbon/LMO and (b) MSNP-LTO/LMO cells. Overcharge test showing surface temperature and voltage of (c) carbon/LMO and (d) MSNP-LTO/LMO cells. Reproduced with permission.[4]

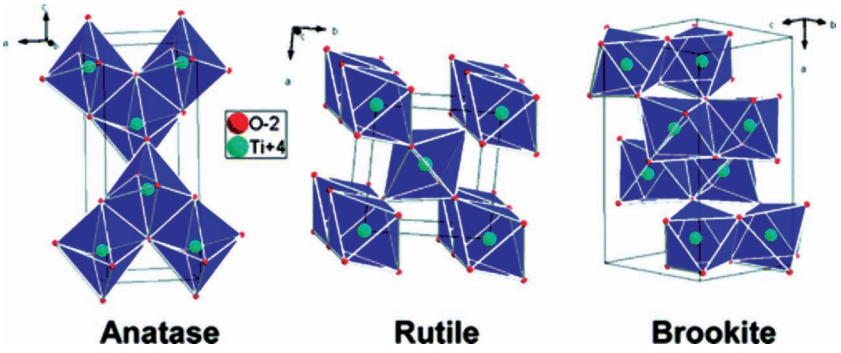

Figure 7. Representations of the anatase, rutile, and brookite forms of TiO_2. Reproduced with permission.[17] Copyright 2010, The American Chemical Society.

structure, which is speculated to cause the irreversible capacity loss of rutile TiO_2 at high lithium content.[41] Therefore, good electrochemical performance was only reported for $Li_xTiO_2$with low degree of lithiation (x<0.5, or reversible capacity smaller than 165 mAh/g).[23] Borghols et al.[42] investigated the lithium insertion mechanism of anatase TiO_2 and found that Li_xTiO_2 (x > 0.5) had poor lithium mobility, and hence, further lithium insertion could only be achieved in the surface layer (<4 nm). Hence, considerable research has been devoted to synthesis routes for nanostructured TiO_2 with the goal to improve the electrochemical performance by a higher degree of lithium insertion.[19,23,41,43,44]

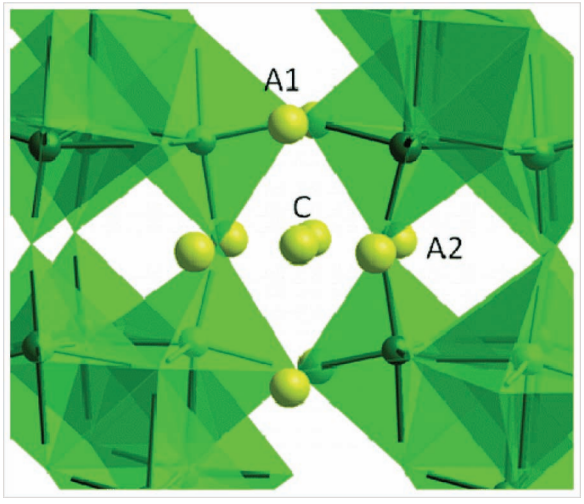

Figure 8. Bulk crystal structure of TiO_2(B) showing TiO_6 octahedra and lithium insertion sites. Reproduced with permission.[39] Copyright 2010, The American Chemical Society.

Mesoporous TiO_2 anode materials with large secondary particle size are being developed as anode material to take advantage of the good electrochemical performance of nanometer-sized TiO_2 and the high tap density of micrometer-sized materials.[21,22] **Figure 10** shows the electrochemical performance of mesoporous nano-structured anatase TiO_2 as the anode material in half cells; these materials were prepared by a urea-assisted hydrothermal method.[21] Figure 10a depicts the voltage profiles during initial charge/discharge cycling of mesoporous TiO_2 materials calcined at different temperatures. The mesoporous TiO_2 calcined at 400 °C delivered a charge capacity (Li extraction) of 164 mAh/g and retained a capacity of 154 mAh/g (94.5% capacity retention) at the end of the 80th cycle (see Figure 10b). However, the mesoporous TiO_2 calcined at 500 °C showed enhanced capacity retention at the expense of slightly reduced specific capacity (147 mAh/g). This finding may be attributed to the particle growth at the elevated temperature. Figure 10c shows the voltage profiles of a half cell using mesoporous TiO_2 calcined at 400 °C. The cell was discharged to 1.5 V vs. Li^+/Li with a constant current of 1C, and was charged to 3.0 V at currents ranging from C/5 to 20C. The specific charge capacity was 162 mAh/g at the C/2 rate, which is slightly reduced in comparison to 160, 154, and 147 mAh/g attained at the 1, 5, and 10C rates, respectively (see Figure 10d).

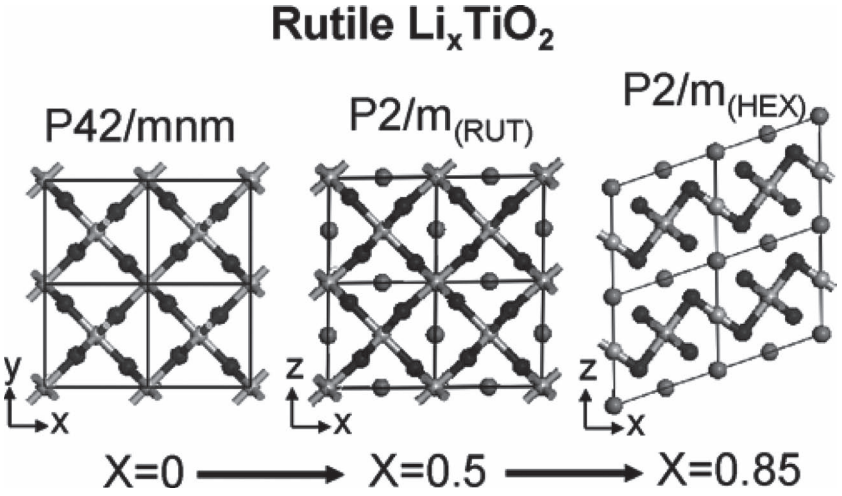

Figure 9. Structural evolution of nano-needle rutile TiO_2 upon lithiation, where x indicates the composition (Li_xTiO_2). Reproduced with permission.[41] Copyright 2008, The American Chemical Society.

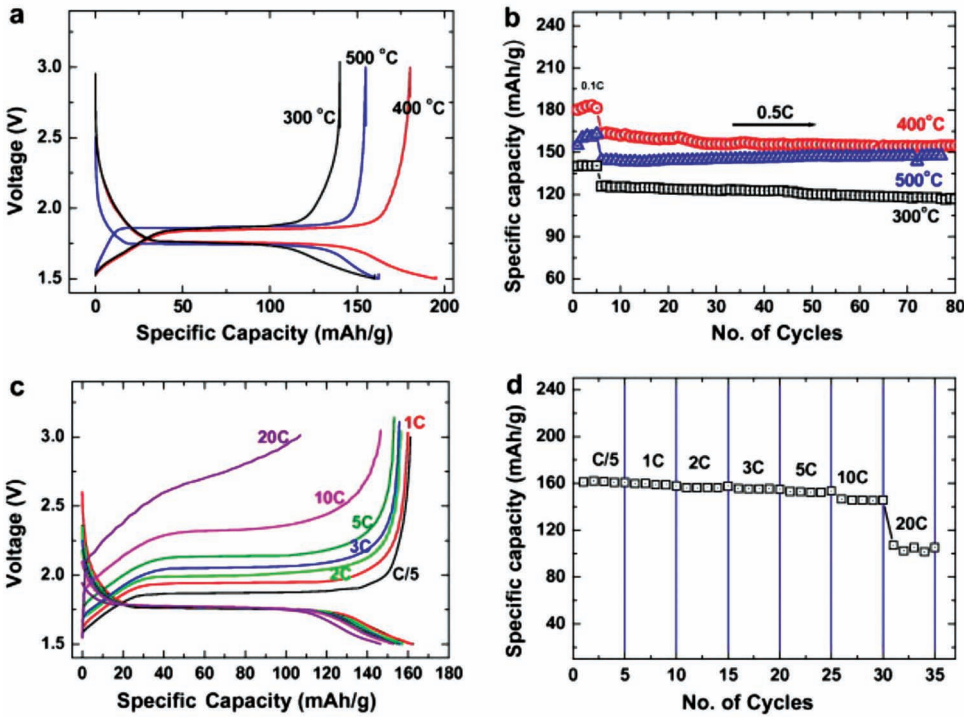

Figure 10. (a) Potential vs. capacity and (b) cycle life behavior of TiO_2 calcined at 300, 400, and 500 °C; (c) potential vs. capacity at rates of C/5 to 20C and (d) rate capability behavior of TiO_2 calcined at 400 °C. Reproduced with permission.[21] Copyright 2009, Elsevier.

4. $MLi_2Ti_6O_{14}$ (M = Sr, Ba, and Na)

$MLi_2Ti_6O_{12}$ (M = Sr, Ba, and Na) is another class of titanium-based oxides that is suitable for reversible lithium insertion and is a promising anode material for lithium-ion batteries. Both a solid-state reaction[26] and sol-gel process[24] have been used to prepare $MLi_2Ti_6O_{12}$ (M = Sr, Ba, and Na). **Figure 11** schematically shows the crystal structure of $MLi_2Ti_6O_{14}$, which is built upon the corner and edge sharing of the TiO_6 octahedra, forming layers parallel to the (100) plane. The edge-sharing configuration applies to adjunct TiO_6 octahedra in the same layer, and the corner-sharing configuration applies to TiO_6 octahedra in adjunct layers. Lithium atoms occupy the tetrahedral site between two layers, while divalent M occupies half of the 11-coordinated (where one of the M-O bonds is stretched to 4.15 Å) sites between mirror layers.[45] Hence, the structure for $SrLi_2Ti_6O_{14}$ and $BaLi_2Ti_6O_{14}$ has a space group of Cmca. Replacing the divalent atoms with double the number of Na atoms leads to the full occupation of the 11-coordinated site and high unit cell symmetry (space group Fmmm).

In theory, one unit of $MLi_2Ti_6O_{14}$ can host up to six lithium atoms to completely reduce Ti(IV) to Ti(III), providing a theoretical capacity of about 240 mAh/g (depending on the atomic weight of M). However, the mechanism of lithium insertion into $MLi_2Ti_6O_{14}$ is poorly understood, and only about ¾ of its theoretical capacity has been attained in electrochemical tests. **Figures 12**a, 12b, and 12c show typical voltage profiles for half cells using $SrLi_2Ti_6O_{14}$, $BaLi_2Ti_6O_{14}$, and $Na_2Li_2Ti_6O_{14}$ materials, respectively, as the anode. The cells were charged/discharged between 0.5 V and 2.0 V vs. Li^+/Li with a constant current of 10 mA/g. The initial discharge capacities of the $SrLi_2Ti_6O_{14}$, $BaLi_2Ti_6O_{14}$, and $Na_2Li_2Ti_6O_{14}$ half cells were 145, 118, and 116 mAh/g, respectively, with multiple insertion steps. After post-processing by high-speed ball milling to break down agglomerates, $BaLi_2Ti_6O_{14}$ was able to deliver an initial discharge capacity of

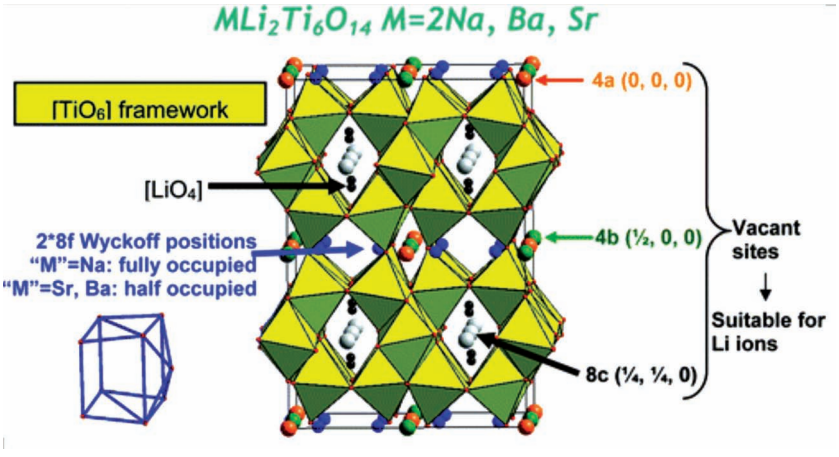

Figure 11. Schematic representation of the $MLi_2Ti_6O_{14}$ structure. Reproduced with permission.[24] Copyright 2012, The American Chemical Society.

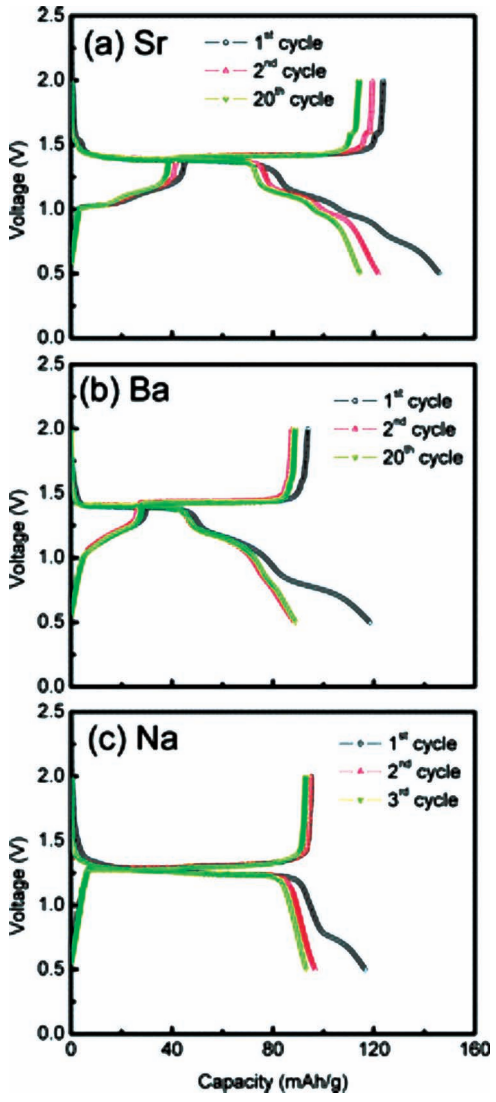

Figure 12. Charge/discharge voltage profiles of (a) $SrLi_2Ti_6O_{14}$, (b) $BaLi_2Ti_6O_{14}$, and (c) $Na_2Li_2Ti_6O_{14}$ electrodes cycled between 0.5 and 2 V at 10 mA/g. Reproduced with permission.[24] Copyright 2012, The American Chemical Society.

about 160 mAh/g.[24] Belharouak et al.[26] investigated the electrochemical performance of $SrLi_2Ti_6O_{14}$ and $BaLi_2Ti_6O_{14}$, both of which were prepared by solid-state synthesis (electrode materials for the test results shown in Figure 12 were prepared by the sol-gel approach). Both $MLi_2Ti_6O_{12}$ materials delivered an initial capacity of more than 150 mAh/g, and capacity retention was good for up to 40 cycles for these materials when tested within the voltage window between 0.5 V and 2.0 V vs. Li^+/Li with a constant current of C/7.

5. Closing Remarks

In brief, great progress has been made in developing titanium-based anode materials ($Li_4Ti_5O_{12}$, TiO_2, and $MLi_2Ti_6O_{14}$) for applications in hybrid electric vehicles. In general, these high-power materials show improved tolerance to thermal abuse compared with the conventional graphite anode.

The synthesis route to prepare nano-structured $Li_4Ti_5O_{12}$ is well established. Bulk $Li_4Ti_5O_{12}$ with micrometer-sized particles has low specific capacity and poor rate capability due to the difficulty of lithium migration from the 8a to 16c sites in bulk materials. However, this issue can be resolved by taking advantage of the boundary effect of nano-structured materials. It has been consistently reported that lithium-ion batteries using nano-structured $Li_4Ti_5O_{12}$ as the anode have extremely long cycle life and calendar life, high power capability, and unmatched safety characteristics. As a quick example, **Table 1** compares the performance of a battery pack using $Li_{1+x}Mn_{2-x}O_4$ as the cathode and $Li_4Ti_5O_{12}$ with micrometer-sized secondary particles and nanometer-sized primary particles as the anode against the technical requirements for hybrid electric vehicles proposed by FreedomCAR.[5] The data clearly show that this exemplary lithium-ion chemistry has already exceeded all the technical requirements needed. Furthermore, it has recently been reported that $Li_4Ti_5O_{12}$ is also an ideal candidate as the anode electrolyte for extremely large-scale and low-cost viscous flow batteries due to its long life and excellent safety performance.[46] However, $Li_4Ti_5O_{12}$ has an intrinsic gassing issue associated with lithiated $Li_{4+x}Ti_5O_{12}$ that is rarely mentioned in the open literature. The lithiated $Li_{4+x}Ti_5O_{12}$ has a tendency to

Table 1. Gap analysis comparing the performance of MSNP-LTO/LMO battery pack and HEV battery pack in terms of PNGV requirements.

	HEV battery requirement	MSNP-LTO/LMO battery pack performance based on BSF 112
Pulse discharge power (10 s)	25 kW	32.66 kW
Peak regenerative peak power (10 s)	20 kW, 55 Wh-pulse	26.13 kW
Total available energy	0.3 kWh at C/1 rate	0.43 kWh
Minimum round-trip energy efficiency	90% 25-Wh cycle	97%
Cold cranking power at –30 °C	5 kW	5 kW
Maximum weight	40 kg	12 kg
Maximum volume	32 L	8.9 L
Maximum allowable self-discharge rate	50 Wh/day	1 Wh/day
Equipment operation temperature range	–30 to +52 °C	–30 to +55 °C

react with non-aqueous electrolyte and generate gas when aged at elevated temperatures. Resolving the gassing issue would enable the successful deployment of the $Li_4Ti_5O_{12}$ anode.

Compared to $Li_4Ti_5O_{12}$, TiO_2 and $MLi_2Ti_6O_{14}$ (M = Sr, Ba, and Na) have similar reversible capacity, around 140–170 mAh/g, and good capacity retention. Lithium uptake is 0.6 Li per Ti for $Li_4Ti_5O_{12}$, about 0.5 Li per Ti for TiO_2, and about 0.5 Li per Ti for $MLi_2Ti_6O_{14}$. The dramatic crystal structure change upon lithium insertion into TiO_2 makes it inferior to $Li_4Ti_5O_{12}$, a zero strain material. The insertion mechanism of $MLi_2Ti_6O_{14}$ has not been systematically studied yet, but a simple comparison indicates that the capacity retention of $MLi_2Ti_6O_{14}$ is also inferior to that of $Li_4Ti_5O_{12}$. It is clear that TiO_2 and $MLi_2Ti_6O_{14}$ can uptake more lithium by reducing their operating potential, which is typically lower than 0.8 V vs. Li^+/Li. However, the utilization of this portion of storage capacity will thermodynamically trigger the decomposition of the carbonate solvents in the electrolyte and the formation of a conventional SEI layer that can result in thermal instability. Hence, this portion of extra capacity is less attractive from the perspective of battery safety.

Acknowledgements

Research funded by the U.S. Department of Energy, FreedomCAR and Vehicle Technologies Office. Argonne National Laboratory is operated for the U.S. Department of Energy by UChicago Argonne, LLC, under contract DE-AC02-06CH11357. This work was also supported by the Human Resources Development of the Korea Institute of Energy Technology Evaluation and Planning (KETEP) grant funded by the Korea government Ministry of Knowledge Economy (No. 20104010100560). The authors also acknowledge EnerDel for fruitful collaboration.This article was amended after online publication to designate Prof. Sun as a corresponding author.

Received: March 13, 2012
Published online: July 25, 2012

[1] J. B. Goodenough, H. D. Abruña, M. V. Buchanan, Basic Research Needs for Electric Energy Storage: Report of the Basic Energy Sciences Workshop on Electrical Energy Storage (U.S. Department of Energy, *Office of Basic Energy Sciences*, Washington, DC, **2007**).
[2] G. Jeong, Y. U. Kim, H. Kim, Y. J. Kim, H. J. Sohn, *Energy Environ. Sci.* **2011**, *4*, 1986–2002.
[3] S. Y. Chung, J. T. Bloking, Y. M. Chiang, *Nat. Mater.* **2002** *1*, 123–128.
[4] K. Amine, I. Belharouak, Z. H. Chen, T. Tran, H. Yumoto, N. Ota, S. T. Myung, Y. K. Sun, *Adv. Mater.* **2010**. *22*, 3052–3057.
[5] Partnership of New Generation Vehicle Battery Test Manual, revision 3. 2001: US Department Of Energy.
[6] H. J. Bang, H. Joachin, H. Yang, K. Amine, J. Prakash, *J. Electrochem. Soc.* **2006**, *153*, A731–A737.
[7] I. Belharouak, W. Q. Lu, D. Vissers, K. Amine, *Electrochem. Commun.* **2006**, *8*, 329–335.
[8] M. Holzapfel, F. Alloin, R. Yazami, *Electrochim. Acta* **2004**, *49*, 581–589.
[9] S. Flandrois, B. Simon, *Carbon* **1999**, *37*, 165–180.
[10] Z. H. Chen, Y. Qin, Y. Ren, W. Q. Lu, C. Orendorff, E. P. Roth, K. Amine, *Energy Environ. Sci.* **2011**, *4*, 4023–4030.
[11] I. Belharouak, Y. K. Sun, W. Lu, K. Amine, *J. Electrochem. Soc.* **2007**, *154*, A1083–A1087.
[12] J. W. Jiang, J. Chen, J. R. Dahn, *J. Electrochem. Soc.* **2004**, *151*, A2082–A2087.
[13] H. G. Jung, S. T. Myung, C. S. Yoon, S. B. Son, K. H. Oh, K. Amine, B. Scrosati, Y. K. Sun, *Energy Environ. Sci.* **2011**, *4*, 1345–1351.
[14] W. Lu, I. Belharouak, J. Liu, K. Amine, *J. Power Sources* **2007**, *174*, 673–677.
[15] W. Lu, I. Belharouak, J. Liu, K. Amine, *J. Electrochem. Soc.* **2007**, *154*, A114–A118.
[16] H. M. Wu, I. Belharouak, H. Deng, A. Abouimrane, Y. K. Sun, K. Amine, *J. Electrochem. Soc.* **2009**, *156*, A1047–A1050.
[17] D. Dambournet, I. Belharouak, K. Amine, *Chem. Mater.* **2010**, *22*, 1173–1179.
[18] D. Dambournet, I. Belharouak, J. W. Ma, K. Amine, *J. Mater. Chem.* **2011**, *21*, 3085–3090.
[19] D. Dambournet, K. W. Chapman, P. J. Chupas, R. E. Gerald, N. Penin, C. Labrugere, A. Demourgues, A. Tressaud, K. Amine, *J. Am. Chem. Soc.* **2011**, *133*, 13240–13243.
[20] D. Dambournet, K. W. Chapman, M. V. Koudriachova, P. J. Chupas, I. Belharouak, K. Amine, *Inorg. Chem.* **2011**, *50*, 5855–5860.
[21] H. G. Jung, S. W. Oh, J. Ce, N. Jayaprakash, Y. K. Sun, *Electrochem. Commun.* **2009**, *11*, 756–759.
[22] H. G. Jung, C. S. Yoon, J. Prakash, Y. K. Sun, *J. Phys. Chem. C* **2009**, *113*, 21258–21263.
[23] S. T. Myung, N. Takahashi, S. Komaba, C. S. Yoon, Y. K. Sun, K. Amine, H. Yashiro, *Adv. Funct. Mater.* **2011**, *21*, 3231–3241.
[24] D. Dambournet, I. Belharouak, K. Amine, *Inorg. Chem.* **2010**, *49*, 2822–2826.
[25] D. Dambournet, I. Belharouak, J. W. Ma, K. Amine, *J. Power Sources* **2011**, *196*, 2871–2874.
[26] I. Belharouak, K. Amine, *Electrochem. Commun.* **2003**, *5*, 435–438.
[27] A. R. Moodenba, D. C. Johnston, R. Viswanat, *Mater. Res. Bull.* **1974**, *9*, 1671–1676.
[28] K. M. Colbow, J. R. Dahn, R. R. Haering, *J. Power Sources* **1989**, *26*, 397–402.
[29] L. Aldon, P. Kubiak, M. Womes, J. C. Jumas, J. Olivier-Fourcade, J. L. Tirado, J. I. Corredor, C. P. Vicente, *Chem. Mater.* **2004**, *16*, 5721–5725.
[30] A. Laumann, H. Boysen, M. Bremholm, K. T. Fehr, M. Hoelzel, M. Holzapfel, *Chem. Mater.* **2011**, *23*, 2753–2759.
[31] W. J. H. Borghols, M. Wagemaker, U. Lafont, E. M. Kelder, F. M. Mulder, *J. Am. Chem. Soc.* **2009**, *131*, 17786–17792.
[32] A. J. Smith, J. C. Burns, D. Xiong, J. R. Dahn, *J. Electrochem. Soc.* **2011**, *158*, A1136–A1142.
[33] D. J. Xiong, J. C. Burns, A. J. Smith, N. Sinha, J. R. Dahn, *J. Electrochem. Soc.* **2011**, *158*, A1431–A1435.
[34] K. Amine, Z. H. Chen, Z. Zhang, J. Liu, W. Q. Lu, Y. Qin, J. Lu, L. Curtis, Y. K. Sun, *J. Mater. Chem.* **2011**, *21*, 17754–17759.
[35] J. H. Jung, H. Kobayashi, K. J. C. van Bommel, S. Shinkai, T. Shimizu, *Chem. Mater.* **2002**, *14*, 1445–1447.
[36] M. C. Tsai, J. C. Chang, H. S. Sheu, H. T. Chiu, C. Y. Lee, *Chem. Mater.* **2009**, *21*, 499–505.
[37] D. Gong, C. A. Grimes, O. K. Varghese, W. C. Hu, R. S. Singh, Z. Chen, E. C. Dickey, *J. Mater. Res.* **2001**, *16*, 3331–3334.
[38] T. Kasuga, M. Hiramatsu, A. Hoson, T. Sekino, K. Niihara, *Adv. Mater.* **1999**, *11*, 1307–1311.
[39] A. R. Armstrong, C. Arrouvel, V. Gentili, S. C. Parker, M. S. Islam, P. G. Bruce, *Chem. Mater.* **2010**, *22*, 6426–6432.
[40] L. Brohan, R. Marchand, *Solid State Ionics* **1983**, *9–10*, 419–424.
[41] W. J. H. Borghols, M. Wagemaker, U. Lafont, E. M. Kelder, F. M. Mulder, *Chem. Mater.* **2008**, *20*, 2949–2955.
[42] W. J. H. Borghols, D. Lutzenkirchen-Hecht, U. Haake, E. R. H. van Eck, F. M. Mulder, M. Wagemaker, *Phys. Chem. Chem. Phys.* **2009**, *11*, 5742–5748.
[43] M. Wagemaker, W. J. H. Borghols, E. R. H. van Eck, A. P. M. Kentgens, G. L. Kearley, F. M. Mulder, *Chem.-Eur. J.* **2007**, *13*, 2023–2028.
[44] M. Wagemaker, W. J. H. Borghols, F. M. Mulder, *J. Am. Chem. Soc.* **2007**, *129*, 4323–4327.
[45] I. Koseva, P. Peshev, S. Pechev, P. Gravereau, J. P. Chaminade, *Zeitschrift Fur Naturforschung Section B-a J. Chem. Sci.*, **2002**, *57*, 512–518.
[46] M. Duduta, B. Ho, V. C. Wood, P. Limthongkul, V. E. Brunini, W. C. Carter, Y. M. Chiang, *Adv. Energy Mater.* **2011**, *1*, 511–516.